Engineered Science
DOI: https://dx.doi.org/10.30919/es1841

Semi-analytical Modeling and Vibration Characteristics Analysis of Functionally Graded Materials Plates on Winkler-Pasternak Elastic Foundations

Xianghong Huang,[1] Luyue Xi,[1] Cong Gao,[1,2,*] Yuchen Fan[1] and Yuan Zhou[1]

Abstract

This study develops a semi-analytical formulation for analyzing the dynamic behaviors of functionally graded plates resting on Winkler-Pasternak elastic foundations. To begin with, the energy formulations for the plate structure are established through incorporating the domain decomposition approach, the first-order shear deformation theory and artificial spring method. Kinematic admissible functions are constructed by the superposition of orthogonal Jacobi polynomials, and the functionally graded materials exhibit continuous property variation along the thickness direction is mathematically defined. Subsequent implementation of the Rayleigh-Ritz variational principle enables systematic resolution of free and forced vibrational behaviors, and the Newmark-β integration approach is used to solve the time domain vibration response of the structure, while validation studies demonstrate exceptional consistency with benchmark solutions from the existing literatures. Ultimately, the influence of the characteristic parameters such as boundary conditions, construction parameters, foundation parameters, and power-law distribution on the dynamic behavior is carried out.

Keywords: Semi-analytical method; Functionally graded plates; Winkler-Pasternak elastic foundations; Orthogonal polynomials; Vibration characteristics.

Received: 18 June 2025; Revised: 15 October 2025; Accepted: 27 October 2025.
Article type: Research article.

1. Introduction

Plate structures have garnered significant research attention in engineering applications owing to their geometrically symmetric configuration and superior structural performance,[1,2] such as construction (bridge deck and structural support system) and ship engineering (deck, bulkhead and stepped baseplate). The superior mechanical properties of functionally graded materials (FGM), including enhanced strength, rigidity, and environmental compatibility, make them particularly suitable for these structural applications.[3-5] In addition, the effects of elastic foundations make the dynamic behaviors of the structure more complex, often resulting in dangerous harmonic vibration, thus damaging the components.[6-8] Investigating the vibrational behavior of FGM plates resting on Winkler-Pasternak foundations holds significant practical importance, particularly for engineering applications requiring advanced material-structure interactions. By selecting the appropriate material parameters and thickness distribution, the dynamic performance of the structure can be grasped, and the weight and cost of the structure are reduced.

Much effort has been dedicated to research the dynamic characteristics of homogeneous plate in recent years. Kolarevic *et al*.[9] explored the dynamic characteristics of rectangular Mindlin plate employing the dynamic stiffness method, and the dynamic stiffness matrix was induced by applying the projection method and the superposition method. Kirisik and Yueksel conducted a dynamic analysis on the rectangular plate under Kelvin type edge restraints utilizing the separation variables approach.[10] To obtain the stable solution of the cantilever plates, Wu *et al*.[11] used the mixed variables principle to analyze the dynamic behaviors of the rectangular plate under uniform load. According to the

[1] *School of Naval Architecture & Ocean Engineering, Jiangsu University of Science and Technology, Zhenjiang, 212001, China*
[2] *College of Shipbuilding Engineering, Harbin Engineering University, Harbin, 150001, China*
**E-mail:* conggao@hrbeu.edu.cn (C. Gao)

Kirchhoff theory, Lü *et al*.[12] solved the natural frequencies of rectangular plates under general edge restraints through adopting the Differential Quadrature Method, and discussed the influence of the internal support position and the mixed edge restraints. Ramu and Mohanty calculated the stiffness matrix and mass matrix of Kirchhoff plate by using Finite element method,[13] and the results of the simply supported rectangular plate were in good agreement with the exact solution results. Kwak and Han introduced the independent coordinate coupling method (ICCM) for dynamic analysis of plates with holes,[14] simplifying energy calculations and improving the construction of mass and stiffness matrices. Kim *et al*.[15] proposed an assumed mode approach for dynamic analysis of rectangular plates with arbitrary edge constraints, showing good agreement with other methods like finite element analysis and analytic solutions. Zhao *et al*.[16,17] derivated the vibroacoustic response of plates by using the Chebyshev spectral method and Helmholtz boundary integral equation, the effects of structural shape, free surface and immersed depths on structural acoustic radiation were explored. Singhatanadgid and Taranajetsada carried out the vibration behaviors of variable thickness plates using variational principles and Kantorovich method, providing numerical solutions.[18] For plates on elastic foundations, Su *et al*.[19] obtained the series expansion solution of the dynamic behavior of a rectangular plate clamped on an elastic foundation by using the separation of variables method. Srubshchik *et al*.[20] analyzed the static and dynamic buckling of slender rectangular plate resting on nonlinear elastic foundation, employing asymptotic methods and perturbation theory to derive load formulas and numerical results. Celep *et al*.[21] investigated forced vibration of triangular plates on unilateral Winkler foundations using Chebyshev polynomial and iterative method, revealing significant foundation dominance in static/dynamic responses. Through the Galerkin method, according to Hamilton variation principle, the researches systematically investigated how structural, foundation, and excitation force parameters affect the frequency response behaviors of thin rectangular plates resting on nonlinear elastic foundations.[22,23]

In the realm of dynamic research for composite plates, Hajheidari and Mirdamadi introduced a spectral FEM to explore the free and transient response of laminated plate.[24] Phuc and Khue analyzed the free and forced vibrations of piezoelectric FGM plates on two-parameter elastic foundations in thermal environments,[25] using FEM to examine material, geometric, and environmental effects. Srivastava *et al*.[26,27] developed an efficient meshless method based on the higher-order shear deformation theory for buckling and vibration analysis of FG plates. Singh *et al*.[28] established the artificial neural network-based predictive model for the vibration analysis of FG plates with cut-outs in the framework of the higher-order shear deformation theory. Thinh *et al*.[29] studied the vibrational behavior of a FG rectangular plate submerged in fluid, considering material property variations, fluid-structure interaction, and influencing parameters like boundary conditions, aspect ratios, and fluid depth on natural frequencies. FG plates are frequently analyzed using the first-order shear deformation theory (FSDT) in contemporary research, the effect of transverse shear deformation is considered in FSDT compared with the classical plate theory (CPT), and the calculation variables are reduced for the simplification in FSDT compared with the high-order shear deformation theory (HSDT). Hosseini *et al*.[30] presented analytical solutions for the dynamic analysis of FG plates resting on Winkler or Pasternak foundations, using FSDT to evaluate the effects of edge restraints, foundation stiffness, and material properties on eigenfrequencies. Based on the FSDT and Hamiltonian principle, Javani *et al*.[31] derived the free vibration equation of composite T-shaped plate, in which the motion of each segmentation element is extracted by the finite element part in the generalized differential quadrature element. Ghosh *et al*.[32] employed a 9-noded FEM based on the FSDT to analyze free vibration of laminated composite plates with attached masses on elastic foundations, revealing mass placement at nodes enables tuned damping and foundation-dependent behavioral sh ifts. Pham *et al*.[33-36] developed a modified nonlocal strain gradient theory for multi-scale analysis and established the dynamic model of FG nanoplates, and the influence of geometric dimensions, material gradients, foundation stiffness and damping characteristics on the vibration response was also investigated. Wang *et al*.[37-39] carried out a lot of research on the dynamic characteristics of composite plates under arbitrary edge restraints by using the improved Fourier series method, and the influence of material parameters, structural parameters and boundary parameters on the vibration characteristics of the structure was given.

While extensive studies have been conducted on vibrational analysis of homogeneous and FGM plates, the dynamic response of FGM plates with variable thickness on Winkler-Pasternak elastic foundations remains underexplored. Addressing this knowledge gap, the present investigation develops a semi-analytical model of uniform and stepped FGM plates resting on Winkler-Pasternak elastic foundations combining: Establishing energy formulation through domain decomposition approach, the first-order shear deformation theory and interfacial spring, Rayleigh-Ritz approximation for

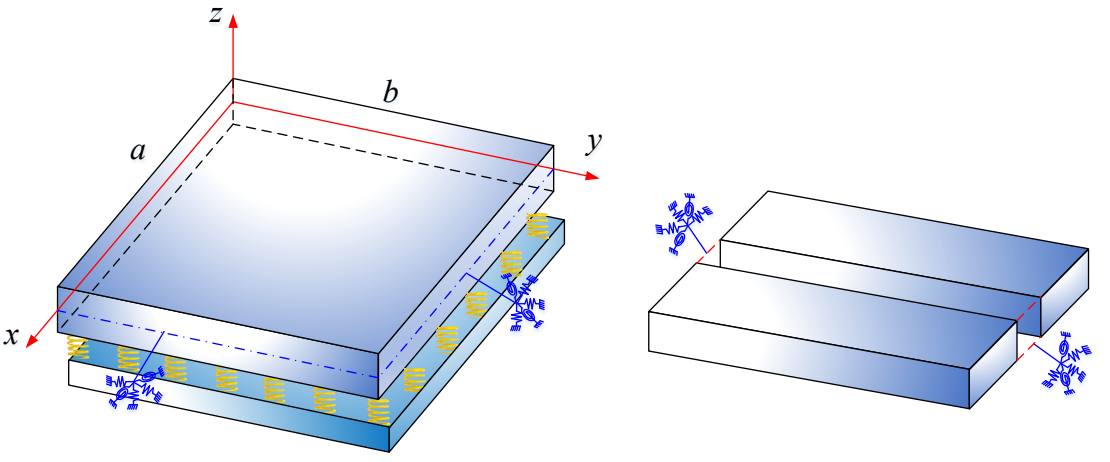

Fig. 1: Calculation model of FGM plate on the Winkler–Pasternak elastic foundation.

mode shape determination, Newmark-β integration approach for time domain vibration response. The displacement admissible functions are represented using orthogonal Jacobi polynomials and trigonometric series, the Chebyshev polynomial, Legendre polynomial and other orthogonal polynomials can be obtained by setting different the Jacobi parameters, which generalizes the selection of admissible displacement functions by using Jacobi polynomials. The proposed methodology undergoes rigorous validation through comparative studies with both published numerical results, thereby establishing a comprehensive understanding of vibration mechanisms in FGM plates.

The structure of this study is organized as follows: Chapter 2 presents the semi-analytical modeling of FGM plate on elastic foundations. In Chapter 3, the comparison analysis and verification study of the current method are carried out. In Chapter 4, we discuss a set of comprehensive numerical examples. Finally, Chapter 5 offers concluding remarks of the study.

2. Semi-analytical modeling of FGM plate on elastic foundations

2.1. Model description

The proposed FGM plate model (Fig. 1), with overall dimensions $a \times b$, employs a Cartesian coordinate system (x, y, z) to define three-dimensional displacement fields. The plate is discretized into N_r longitudinal segments along length direction via the domain decomposition method, where the i-th segment exhibits distinct geometric parameters a_i (length) and h_i (thickness). Resting on a Winkler-Pasternak foundation, the system incorporates spring-based interfaces between adjacent segments to enhance inter-segment coupling fidelity and emulate various boundary constraints.

The FGM plate is considered to be a single-layered plate that is made of ceramic and metal. The material property is assumed to be graded through the thickness in accordance with a power-law distribution. The Young's modulus, Poisson's ratios and mass density of the FGM plate are derived from the law of mixtures in Eqs. (1)-(3):

$$E(z) = (E_c - E_m)V_c + E_m \tag{1}$$

$$\mu(z) = (\mu_c - \mu_m)V_c + \mu_m \tag{2}$$

$$\rho(z) = (\rho_c - \rho_m)V_c + \rho_m \tag{3}$$

where E_c, μ_c, ρ_c represent ceramic constituents and E_m, μ_m, ρ_m represent metallic constituents. The volume fraction V_c of the structure can be shown as the following types, expressed by Eq. (4):[40,41]

$$V_c = \left(\frac{1}{2} + \frac{z}{h}\right)^p \tag{4}$$

where p are the material control parameters, the volume fraction of the FGM plate is illustrated in Fig. 2, with the special case of $p \to 0$ or $p \to \infty$ yielding homogeneous isotropic material behavior.

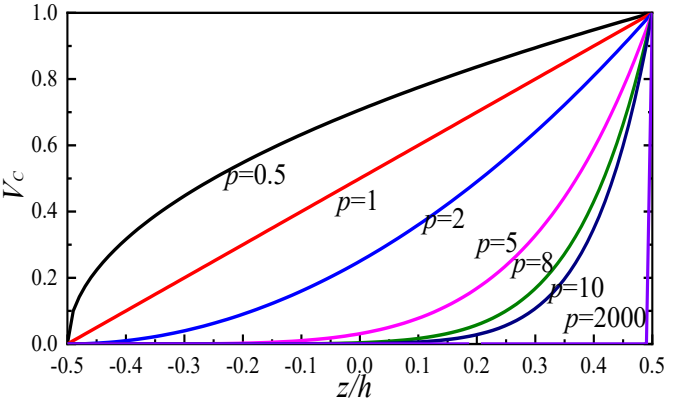

Fig. 2: Variations of the volume fraction (V_c) for different values of power-law exponent p.

2.2 Energy expressions

The combined internal forces and moments of the structure are given by Eqs. (5) and (6):[42]

$$\begin{bmatrix} N_{xx}^i \\ N_{yy}^i \\ N_{xy}^i \\ M_{xx}^i \\ M_{yy}^i \\ M_{xy}^i \end{bmatrix} = \begin{bmatrix} A_{11} & A_{12} & 0 & B_{11} & B_{12} & 0 \\ A_{12} & A_{22} & 0 & B_{12} & B_{22} & 0 \\ 0 & 0 & A_{66} & 0 & 0 & B_{66} \\ B_{11} & B_{12} & 0 & D_{11} & D_{12} & 0 \\ B_{12} & B_{22} & 0 & D_{12} & D_{22} & 0 \\ 0 & 0 & B_{66} & 0 & 0 & D_{66} \end{bmatrix} \begin{bmatrix} \varepsilon_{xx}^{0,i} \\ \varepsilon_{yy}^{0,i} \\ \gamma_{xy}^{0,i} \\ \chi_{xx}^i \\ \chi_{yy}^i \\ \chi_{xy}^i \end{bmatrix} \quad (5)$$

$$\begin{Bmatrix} Q_x^i \\ Q_y^i \end{Bmatrix} = \bar{\kappa} \begin{bmatrix} A_{55} & A_{45} \\ A_{45} & A_{44} \end{bmatrix} \begin{bmatrix} \gamma_{xz}^{0,i} \\ \gamma_{yz}^{0,i} \end{bmatrix} \quad (6)$$

where N_{xx}, N_{yy}, N_{xy}, M_{xx}, M_{yy}, M_{xy}, Q_x and Q_y respectively represent the in-plane force resultants, moment resultants, and transverse shear force resultants. The value of the shear correction factor $\bar{\kappa}$ is 5/6 in this analysis.[43,44] The extensional stiffness A_{ij}, B_{ij} and D_{ij} are defined as follows Eq. (7):[45]

$$(A_{ij}, B_{ij}, D_{ij}) = \int_{-h/2}^{h/2} Q_{ij}(z)(1, z, z^2)dz \quad (7)$$

and the through-thickness varying stiffness component $Q_{ij}(z)$, governing the plate's constitutive behavior, is mathematically expressed as Eq. (8):

$$Q_{11}(z) = Q_{22}(z) = \frac{E(z)}{1-\mu^2(z)}, Q_{12}(z) = \frac{\mu(z)E(z)}{1-\mu^2(z)}, Q_{66}(z) = \frac{E(z)}{2[1+\mu(z)]} \quad (8)$$

Based on the FSDT,[46,47] the strain components of the structure at any point are in Eqs. (9) and (10):

$$\varepsilon_{xx}^i = \varepsilon_{xx}^{0,i} + z\chi_{xx}^i, \ \varepsilon_{yy}^i = \varepsilon_{yy}^{0,i} + z\chi_{yy}^i \quad (9)$$

$$\gamma_{xy}^i = \gamma_{xy}^{0,i} + z\chi_{xy}^i, \ \gamma_{yz}^i = \gamma_{yz}^{0,i}, \ \gamma_{xz}^i = \gamma_{xz}^{0,i} \quad (10)$$

where the specific expressions are expressed as in Eqs. (11)-(13):

$$\varepsilon_{xx}^{0,i} = \frac{\partial u_0^i}{\partial x}, \ \varepsilon_{yy}^{0,i} = \frac{\partial v_0^i}{\partial y} \quad (11)$$

$$\gamma_{xy}^{0,i} = \frac{\partial u_0^i}{\partial y} + \frac{\partial v_0^i}{\partial x}, \ \gamma_{yz}^{0,i} = \frac{\partial w_0^i}{\partial y} + \phi_y^i, \ \gamma_{xz}^{0,i} = \frac{\partial w_0^i}{\partial x} + \phi_x^i \quad (12)$$

$$\chi_{xx}^i = \frac{\partial \phi_x^i}{\partial x}, \ \chi_{yy}^i = \frac{\partial \phi_y^i}{\partial y}, \ \chi_{xy}^i = \frac{\partial \phi_x^i}{\partial y} + \frac{\partial \phi_y^i}{\partial x} \quad (13)$$

The displacement field components (u, v, w) represent plate motions along the (x, y, z) coordinate axes respectively, while (ϕ_x, ϕ_y) denote rotational displacements about these axes. For the i-th structural segment, the strain energy formulation incorporates both bending and stretching components, as follows:[48,49]

Through algebraic combination of Eqs. (5)-(6) and (11)-(13) within Eq. (14), the strain energy can be divided into U_S^i, U_{BC}^i and U_B^i clarified by A_{ij}, B_{ij} and D_{ij} in Eqs. (15)-(17):

$$U_V^i = \frac{1}{2}\int_0^{a/N_r}\int_0^b \left(N_{xx}^i\varepsilon_{xx}^{0,i} + N_{yy}^i\varepsilon_{yy}^{0,i} + N_{xy}^i\gamma_{xy}^{0,i} + M_{xx}^i\chi_{xx}^i + M_{yy}^i\chi_{yy}^i + M_{xy}^i\chi_{xy}^i + Q_x^i\gamma_{xz}^{0,i} + Q_y^i\gamma_{yz}^{0,i}\right)dxdy \quad (14)$$

$$U_S^i = \frac{1}{2}\int_0^{a/N_r}\int_0^b \left\{ \begin{array}{l} A_{11}\left(\frac{\partial u_0^i}{\partial x}\right)^2 + A_{22}\left(\frac{\partial v_0^i}{\partial y}\right)^2 + A_{66}\left(\frac{\partial u_0^i}{\partial y} + \frac{\partial v_0^i}{\partial x}\right)^2 + 2A_{12}\left(\frac{\partial u_0^i}{\partial x}\right)\left(\frac{\partial v_0^i}{\partial y}\right) \\ +\bar{\kappa}A_{44}\left(\frac{\partial w_0^i}{\partial y} + \phi_y^i\right)^2 + \bar{\kappa}A_{55}\left(\frac{\partial w_0^i}{\partial x} + \phi_x^i\right)^2 + 2\bar{\kappa}A_{45}\left(\frac{\partial w_0^i}{\partial x} + \phi_x^i\right)\left(\frac{\partial w_0^i}{\partial y} + \phi_y^i\right) \end{array} \right\} dxdy \quad (15)$$

$$U_{BS}^i = \frac{1}{2}\int_0^{a/N_r}\int_0^b \left\{ \begin{array}{l} B_{11}\left(\frac{\partial u_0^i}{\partial x}\right)\left(\frac{\partial \phi_x^i}{\partial x}\right) + B_{12}\left[\left(\frac{\partial u_0^i}{\partial x}\right)\left(\frac{\partial \phi_y^i}{\partial y}\right) + \left(\frac{\partial v_0^i}{\partial y}\right)\left(\frac{\partial \phi_x^i}{\partial x}\right)\right] \\ +B_{22}\left(\frac{\partial v_0^i}{\partial y}\right)\left(\frac{\partial \phi_y^i}{\partial y}\right) + B_{66}\left(\frac{\partial v_0^i}{\partial x} + \frac{\partial u_0^i}{\partial y}\right)\left(\frac{\partial \phi_x^i}{\partial y} + \frac{\partial \phi_y^i}{\partial x}\right) \end{array} \right\} dxdy \quad (16)$$

$$U_B^i = \frac{1}{2}\int_0^{a/N_r}\int_0^b \left\{ \begin{array}{l} D_{11}\left(\frac{\partial \phi_x^i}{\partial x}\right)^2 + 2D_{12}\left(\frac{\partial \phi_x^i}{\partial x}\right)\left(\frac{\partial \phi_y^i}{\partial y}\right) \\ +D_{22}\left(\frac{\partial \phi_y^i}{\partial y}\right)^2 + D_{66}\left(\frac{\partial \phi_x^i}{\partial y} + \frac{\partial \phi_y^i}{\partial x}\right) \end{array} \right\} dxdy \quad (17)$$

$$U_b = \frac{1}{2}\int_0^b \begin{Bmatrix} \left[k_{u,x0}u_0^2 + k_{v,x0}v_0^2 + k_{w,x0}w_0^2 + k_{x,x0}\phi_x^2 + k_{y,x0}\phi_y^2\right]_{x=0} \\ +\left[k_{u,xL}u_0^2 + k_{v,xL}v_0^2 + k_{w,xL}w_0^2 + k_{x,xL}\phi_x^2 + k_{y,xL}\phi_y^2\right]_{x=a} \end{Bmatrix} dy + \frac{1}{2}\int_0^a \begin{Bmatrix} \left[k_{u,y0}u_0^2 + k_{v,y0}v_0^2 + k_{w,y0}w_0^2 + k_{x,y0}\phi_x^2 + k_{y,y0}\phi_y^2\right]_{y=0} \\ +\left[k_{u,yL}u_0^2 + k_{v,yL}v_0^2 + k_{w,yL}w_0^2 + k_{x,yL}\phi_x^2 + k_{y,yL}\phi_y^2\right]_{y=b} \end{Bmatrix} dx \tag{18}$$

The artificial spring technique employs five distinct spring sets (k_u, k_v, k_w, k_x, k_y) to model boundary constraints in FGM plates, different boundary conditions can be obtained by setting different stiffness values to the spring, while connective springs ensure robust segment coupling. The springs potential energy U_b reserved in the boundary can be expressed as Eq. (18):[50]

Likewise, since the structure is segmented along the x direction, the stored energy in y-axis oriented connective springs can be mathematically expressed through Eq. (19):

$$U_s^i = \frac{1}{2}\int_0^b \begin{Bmatrix} k_u\left(u_0^i - u_0^{i+1}\right)^2 + k_v\left(v_0^i - v_0^{i+1}\right)^2 + k_w\left(w_0^i - w_0^{i+1}\right)^2 \\ +k_x\left(\phi_x^i - \phi_x^{i+1}\right)^2 + k_y\left(\phi_y^i - \phi_y^{i+1}\right)^2 \end{Bmatrix}_{i,i+1} dy \tag{19}$$

The role of the two-parameter Winkler-Pasternak elastic foundation can be described as the stored potential energy U_{es} in Eq. (20):

$$U_{es}^i = \frac{1}{2}\int_0^b \int_{x_i}^{x_{i+1}} \left\{ k_{wt}w_0^2 + k_{st}\left[\left(\frac{\partial w}{\partial x}\right)^2 + \left(\frac{\partial w}{\partial y}\right)^2\right]\right\} dxdy \tag{20}$$

Introducing the nondimensional parameters Eqs. (21) and (22):

$$\overline{k_{wt}} = k_{wt}a^4 / D_{11}^* \tag{21}$$

$$\overline{k_{st}} = k_{st}a^2 / D_{11}^* \tag{22}$$

and the flexural rigidity is taken as Eqs. (23) and (24):[51]

$$D_{11}^* = B_{11}B_{12}^* + B_{12}B_{11}^* + D_{11} \tag{23}$$

where

$$B_{11}^* = \frac{B_{11}A_{12} - B_{12}A_{11}}{(A_{11})^2 - (A_{12})^2}, B_{12}^* = \frac{B_{12}A_{12} - B_{11}A_{11}}{(A_{11})^2 - (A_{12})^2} \tag{24}$$

where A_{11}, A_{12}, B_{11} and B_{12} are defined in Eq. (7).

Therefore, the system's total potential energy can be mathematically expressed through the following functional relationship in Eq. (25):

$$U_{BS} = U_b + \sum_{i=1}^{N_r-1}(U_s^i + U_{es}^i) \tag{25}$$

For the i-th FGM rectangle plate, the kinetic energy expression is given by Eq. (26):

$$T^i = \frac{1}{2}\int_0^{a/N_r}\int_0^b \begin{Bmatrix} I_1\left[\left(\frac{\partial u_0^i}{\partial t}\right)^2 + \left(\frac{\partial v_0^i}{\partial t}\right)^2 + \left(\frac{\partial w_0^i}{\partial t}\right)^2\right] + I_3\left[\left(\frac{\partial \phi_x^i}{\partial t}\right)^2 + \left(\frac{\partial \phi_y^i}{\partial t}\right)^2\right] \\ +2I_2\left[\left(\frac{\partial u_0^i}{\partial t}\right)\left(\frac{\partial \phi_x^i}{\partial t}\right) + \left(\frac{\partial v_0^i}{\partial t}\right)\left(\frac{\partial \phi_y^i}{\partial t}\right)\right] \end{Bmatrix} dxdy \tag{26}$$

The moment of inertia components for the i-th structure are mathematically expressed as Eq. (27):

$$(I_1, I_2, I_3) = \int_{-h/2}^{h/2} \rho(z)\left(1, z, z^2\right)dz \tag{27}$$

The work done by the external concentrated load acting along the z-axis on the i-th FGM rectangle plate is in Eq. (28):

$$W^i = \int f_{w,i}wdz \tag{28}$$

2.3 Solution procedure

Following the multi-segment partitioning approach, the displacement admissible functions are represented using orthogonal Jacobi polynomials and trigonometric series.[52] The recursive relations for Jacobi polynomials generation are in Eqs. (29)-(31):

$$P_0^{(\alpha,\beta)}(\psi) = 1 \tag{29}$$

$$P_1^{(\alpha,\beta)}(\psi) = \frac{\alpha+\beta+2}{2}\psi - \frac{\alpha-\beta}{2} \tag{30}$$

where $\psi \in [-1,1]$, $\alpha, \beta > -1$.

$$P_i^{(\alpha,\beta)}(\psi) = \frac{(\alpha+\beta+2i-1)\left\{\alpha^2 - \beta^2 + \psi(\alpha+\beta+2i)(\alpha+\beta+2i-2)\right\}}{2i(\alpha+\beta+i)(\alpha+\beta+2i-2)}P_{i-1}^{(\alpha,\beta)}(\psi) - \frac{(\alpha+i-1)(\beta+i-1)(\alpha+\beta+2i)}{i(\alpha+\beta+i)(\alpha+\beta+2i-2)}P_{i-2}^{(\alpha,\beta)}(\psi) \qquad i = 2,3..... \tag{31}$$

The structural displacement field components can be defined as Eqs. (32)-(36):

$$u_0 = \sum_{m=0}^{M}\sum_{n=0}^{N} A_m P_m^{(\alpha,\beta)}(x)\cos(\frac{n\pi y}{b})e^{i\omega t} \quad (32)$$

$$v_0 = \sum_{m=0}^{M}\sum_{n=0}^{N} B_m P_m^{(\alpha,\beta)}(x)\sin(\frac{n\pi y}{b})e^{i\omega t} \quad (33)$$

$$w_0 = \sum_{m=0}^{M}\sum_{n=0}^{N} C_m P_m^{(\alpha,\beta)}(x)\sin(\frac{n\pi y}{b})e^{i\omega t} \quad (34)$$

$$\phi_x = \sum_{m=0}^{M}\sum_{n=0}^{N} D_m P_m^{(\alpha,\beta)}(x)\sin(\frac{n\pi y}{b})e^{i\omega t} \quad (35)$$

$$\phi_y = \sum_{m=0}^{M}\sum_{n=0}^{N} E_m P_m^{(\alpha,\beta)}(x)\cos(\frac{n\pi y}{b})e^{i\omega t} \quad (36)$$

where parameters m and n denote the mode number along the x and y direction; M and N represent the polynomial truncation orders.

The complete Lagrangian formulation for the elastic foundations FGM plates system is in Eq. (37):

$$\mathrm{L} = \sum_{1}^{N_e-1}\left(W^i + T^i - U_V^i\right) - U_{BS} \quad (37)$$

The unknown coefficients are determined through variational minimization of the Lagrangian energy functional following Rayleigh-Ritz procedure in Eq. (38):

$$\frac{\partial \mathrm{L}}{\partial \vartheta} = 0 \qquad \vartheta = A_m, B_m, C_m, D_m, E_m \quad (38)$$

The eigenfrequency and dynamic response of the FGM plate is governed by the following characteristic equation (Eq. 39):

$$\left(\mathbf{K} - \omega^2\mathbf{M}\right)\mathbf{Q} = \mathbf{F} \quad (39)$$

The system matrices are defined as: **K** (stiffness), **M** (mass), **Q** (coefficients) and **F** (external excitation).

Time-domain analysis of the FGM plate is conducted employing the Newmark-β numerical integration approach. The structural damping matrix is introduced in Eq. (40):[53]

$$\mathbf{C} = a^*\mathbf{M} + b^*\mathbf{K} \quad (40)$$

where a^* and b^* are Rayleigh damping and set as: a^*=2, b^*=0.00003 in this study.

Assuming that the acceleration is constant in the time range of [t, t+Δt], two parameters β^* and γ^* are introduced:

$$\Delta\ddot{x}_i = \left[\left(1-\beta^*\right)\ddot{x}_i + \beta^*\ddot{x}_{i+1}\right]\Delta t \quad (41)$$

$$\Delta x_i = \dot{x}_i\Delta t + \left[\left(\frac{1}{2}-\gamma^*\right)\ddot{x}_i + \gamma^*\ddot{x}_{i+1}\right]\Delta t^2 \quad (42)$$

where β^*=1/2 and γ^*=1/4 in this study, thus Eqs. (41) and (42) can be represented as Eqs. (43) and (44):

$$\ddot{x}_{i+1} = \frac{1}{\gamma^*\Delta t^2}\Delta x_i - \frac{1}{\gamma^*\Delta t}\dot{x}_i - \left(\frac{1}{2\gamma^*}-1\right)\ddot{x}_i \quad (43)$$

$$\dot{x}_{i+1} = \frac{\beta^*}{\gamma^*\Delta t}\Delta x_i - \left(1-\frac{\beta^*}{\gamma^*}\right)\dot{x}_i + \left(1-\frac{\beta^*}{2\gamma^*}\right)\ddot{x}_i\Delta t \quad (44)$$

The incremental balance equation can be shown as:

$$\mathbf{M}\ddot{x}_{i+1} + \mathbf{C}\dot{x}_{i+1} + \mathbf{K}x_{i+1} = F_{i+1} \quad (45)$$

Eqs. (46)-(48) can be obtained by substituting Eq. (43)- Eq. (44) into Eq. (45):

$$\left[\bar{\mathbf{K}}\right]x_{i+1} = \bar{F}_{i+1} \quad (46)$$

where

$$\left[\bar{\mathbf{K}}\right] = \mathbf{K} + \frac{1}{\gamma^*\Delta t^2}\mathbf{M} + \frac{\beta^*}{\gamma^*\Delta t}\mathbf{C} \quad (47)$$

By repeating the iteration until the end of time, the response of the structure at any time can be obtained.

$$\bar{F}_{i+1} = F_{i+1} + \mathbf{M}\left(\frac{1}{\gamma^*\Delta t^2}x_i + \frac{1}{\gamma^*\Delta t}\dot{x}_i + \left(\frac{1}{2\gamma^*}-1\right)\ddot{x}_i\right) + \mathbf{C}\left(\frac{\beta^*}{\gamma^*\Delta t}x_i + \left(\frac{\beta^*}{\gamma^*}-1\right)\dot{x}_i + \left(\frac{\beta^*}{2\gamma^*}-1\right)\ddot{x}_i\Delta t\right) \quad (48)$$

Table 1: Material properties of the FGM plate.

Properties	Aluminum (Al)	Zirconia (ZrO_2)	Alumina (Al_2O_3)	Ti-6Al-4V
E (GPa)	70	151	380	105.7
ρ (kg/m^3)	2707	3000	3800	4429
μ	0.3	0.3	0.3	0.298

3. Numerical validation

The material properties of the FGM plate is shown in Table 1.[40] Material control parameters p=2, and the convergence is controlled with N_r=4, M=N=8, Jacobi parameters α=β=0. The structural dimensions are a=1 m and b=2 m. For the uniform FGM plate, the overall thickness of the structure is h=0.005 m. For the stepped variable thickness FGM plate, the truncation length of each segment is the same, which is represented by h_i, and the minimum thickness is 0.005 m.

3.1 Convergence and comparison studies

This section conducts numerical simulations to inspect the convergence behavior and veracity of the developed approach. The structural analysis incorporates both linear and rotational spring elements to represent various boundary constraint scenarios. The edge restraints of simply-supported, clamped, elastic supported and free adopting symbols S, C, E and F representations. The spring stiffness parameters are assigned distinct values to represent different boundary constraint scenarios, with the specific numerical values determined as followsm,[39,54] S: k_u=k_v=k_w=10^15 N/m and k_x= k_y=0 , C: k_u =k_v=k_w=k_x=k_y=10^15 Nm/rad, E: k_u =k_v=k_w=k_x=k_y=10^7 Nm/rad, F: k_u =k_v=k_w=k_x=k_y=0.

Fig. 3 systematically examines how natural frequency responds to variations in spring stiffness parameters. The analysis employs a controlled variable approach, maintaining either linear or rotational spring stiffness constant while varying the counterpart. As the rotational spring remains unchanged and the stiffness of the linear spring gradually increases, the curvature of the eigenfrequency of the structure changes slowly. On the contrary, when the linear spring remains unchanged and the stiffness value of the rotational spring increases gradually, the curvature of the eigenfrequency of the structure changes greatly, especially when the spring stiffness is within the range of elastic edge restraints, the eigenfrequency of the structure increases sharply. That is to say, the effect of rotational constraint spring on the eigenfrequency of FGM plate is greater than that of linear constraint spring, therefore, the influence of limiting the rotation angle of the FGM plate on the structural stiffness is more obvious than that of limiting the displacement of the FGM plate.

Fig. 4 displays the convergence of the current method with different truncated number of the polynomial under simply supported on four sides (SSSS) boundary condition and simply supported-clamped-simply supported-clamped (SCSC) boundary condition. Numerical convergence is rapidly achieved with increasing truncation numbers, reaching stability at M=N=6 in the first ten natural frequencies. Therefore, the truncation coefficients are selected as M=N=8 to ensure the robust results in this study.

As mentioned above, by modifying the parameters α and β of Jacobi polynomials, orthogonal polynomials can be transformed into Legendre polynomials, Chebyshev polynomials and other forms of orthogonal polynomials. Taking α=β=0 as the benchmark of comparative analysis,

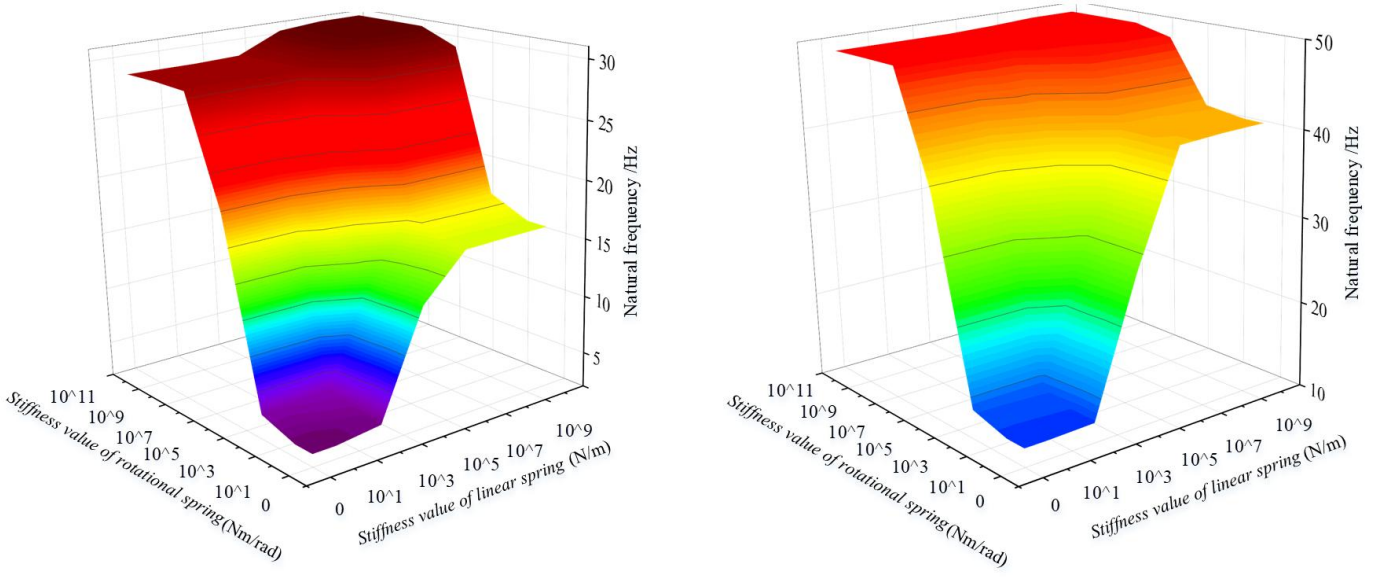

(a) The first order (b) The third order

Fig. 3: Natural frequencies of the structure with different spring stiffness.

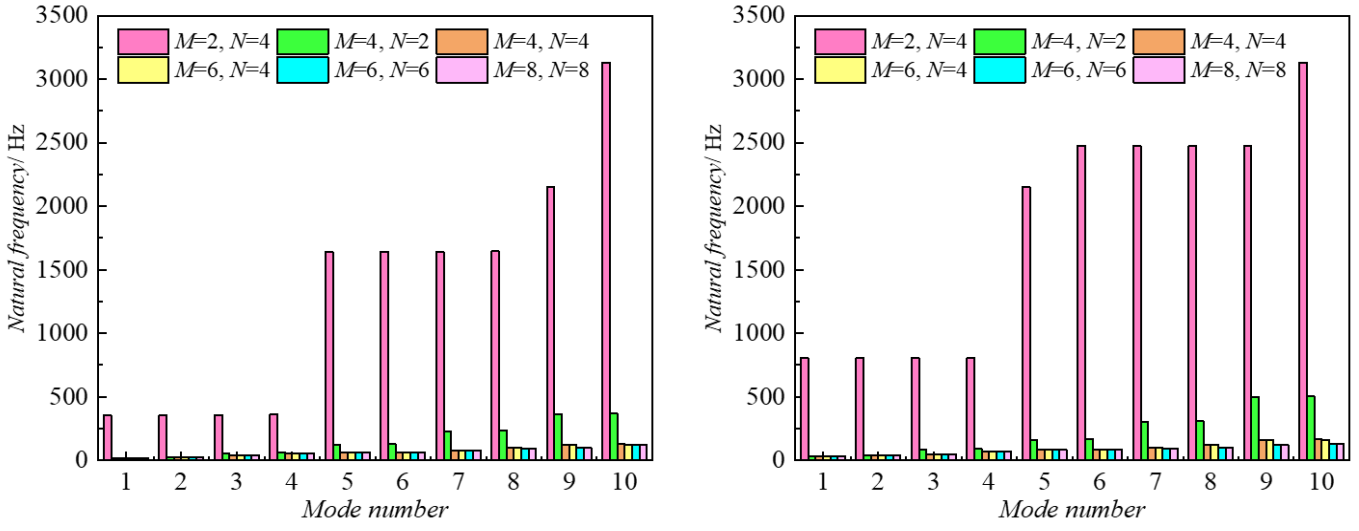

(a) SSSS boundary condition (b) SCSC boundary condition

Fig. 4: Natural frequencies of the structure with different truncated number of the polynomial.

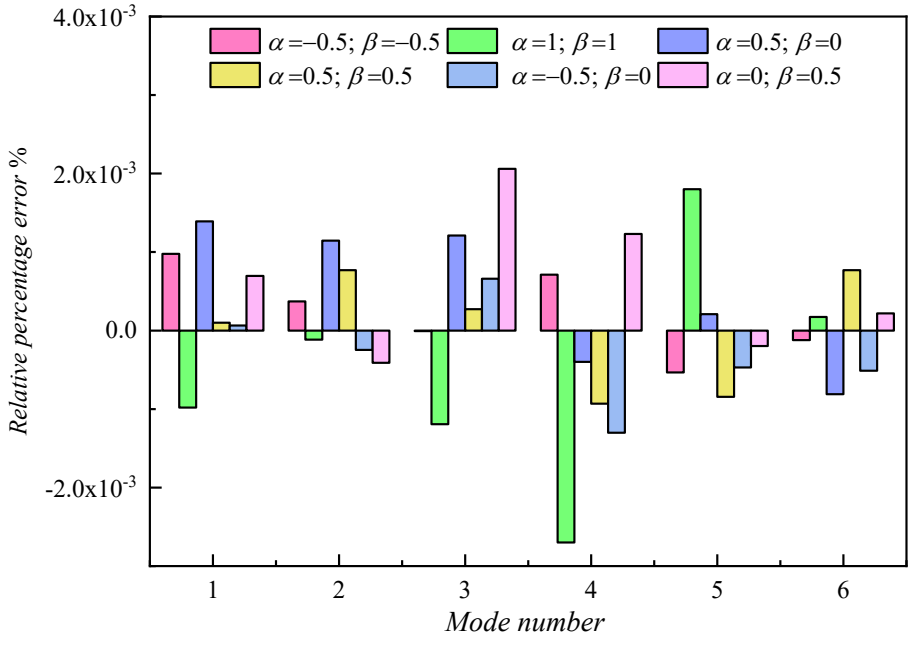

Fig. 5: Relative percentage error with different orthogonal polynomial parameters.

Fig. 5 shows the relative percentage error with different Jacobi parameters. It can be found that the maximum relative percentage error maintains a small margin under different α and β values, that is, the results are stable no matter which Jacobi parameter is selected. A variety of semi-analytical methods with orthogonal polynomials as displacement functions are also unified by using Jacobi polynomials, which highlights the versatility and wide applicability of orthogonal Jacobi polynomials.

3.2 Verification study

Tables 2 and 3 display the frequency parameters of simply supported square FGM plates, with results benchmarked against published literature values. Comparing the present results with those obtained by the CPT, FSDT, 2D HAPT and HSDT shows that all results are in excellent agreement with each other. It is also seen that the present analytical solution for simply supported square Ti-Al-4V/Al FGM plate under consideration provides the results higher than those obtained by the CPT. The present results are lower than those of obtained by the 2D HAPT and HSDT as the plate thickness increases. The comparative analysis confirms the high accuracy of the proposed methodology in predicting vibrational behavior.

Table 2: Comparison of the results for simply supported square Ti-Al-4V/Al FGM plate.

Mode	p=0			p=2000		
	Present	FSDT [40]	CPT [41]	Present	FSDT [40]	CPT [41]
1	144.65	143.67	144.66	270.46	268.60	268.92
2	361.60	360.64	360.53	676.13	674.38	669.40
3	361.60	360.64	360.53	676.13	674.38	669.40
4	577.63	575.87	569.89	1080.07	1076.80	1052.49
5	722.60	725.53	720.57	1351.27	1356.90	1338.52
6	722.60	725.53	720.57	1351.27	1356.90	1338.52
7	937.61	938.18	919.74	1753.30	1754.40	1695.23
8	937.61	938.18	919.74	1753.30	1754.40	1695.23
9	1226.36	1238.76	1225.72	2293.53	2316.90	2280.95
10	1226.36	1238.76	1225.72	2293.53	2316.90	2280.95

Table 3: Comparison of fundamental frequency parameter for simply supported square Al/ZrO_2 plate.

	p=1			h/a=0.2		
	h/a=0.05	h/a=0.1	h/a=0.2	p=2	p=3	p=5
Present	0.0162	0.0621	0.2201	0.2211	0.2220	0.2219
2D HAPT[55]	0.0158	0.0618	0.2285	0.2264	0.2270	0.2281
HSDT[56]	0.0157	0.0613	0.2257	0.2237	0.2243	0.2253

Table 4: Comparison of the fundamental frequency parameter for thin square plate resting on Pasternak elastic foundation.

Boundary conditions	$\overline{k_{wt}}$	$\overline{k_{st}}$	Present	CPT[57]	Mindlin Plate Theory[7]
SSSS	0	0	19.740	19.740	19.739
	0	1000	141.875	141.920	141.876
	1000	0	37.276	37.280	37.278
	1000	1000	145.358	145.430	145.358
SCSC	0	0	28.947	28.950	28.951
	0	1000	146.743	146.730	146.741
	1000	0	42.885	42.870	42.874
	1000	1000	150.110	150.120	150.110
SSSC	0	0	23.643	23.650	23.646
	0	1000	144.213	144.240	144.213
	1000	0	39.498	39.490	39.486
	1000	1000	147.639	147.620	147.639
SCSF	0	0	12.690	12.690	12.686
	0	1000	112.486	112.520	113.315
	1000	0	34.075	34.070	34.073
	1000	1000	116.846	116.920	117.645
SSSF	0	0	11.674	11.680	11.684
	0	1000	111.746	111.710	112.532
	1000	0	33.712	33.710	33.712
	1000	1000	116.133	116.120	116.890

Table 4 presents comparative results of the fundamental frequency parameter for thin square plates on Pasternak foundations, demonstrating excellent agreement between the proposed method and existing solutions. This validation confirms the method's accuracy for vibration analysis of such structural systems.

4. Discussions

4.1 Influence of the boundary condition

Figs. 6 and 7 systematically investigate how different boundary conditions influence both vibrational characteristics in FGM plates. The vibration characteristics of the structure can be observed while fixing the boundary conditions on three sides of the FGM plates and altering the boundary condition solely on the remaining edge. The dynamic response of FGM plates shows significant dependence on boundary conditions under the current spring stiffness, exhibiting progressively enhanced stiffness in the order: F < S < E ≈ C. This progression suggests that strengthening the boundary restraints enhances the structural stiffness.

Figs. 6 and 7 also present the first five modal shapes of FGM plates across different aspect ratios, providing fundamental insights into their free vibration physics. Taking the SCSF boundary condition as an example, it can be observed that the mode shapes exhibit significantly greater prominence along the free edges, and the structural vibration modes with diversity width-to-length ratios are significantly different under the same boundary conditions. More information on the effect of boundary conditions on the free vibration of structures can be seen in Figs. S1 and S2 of Supporting information.

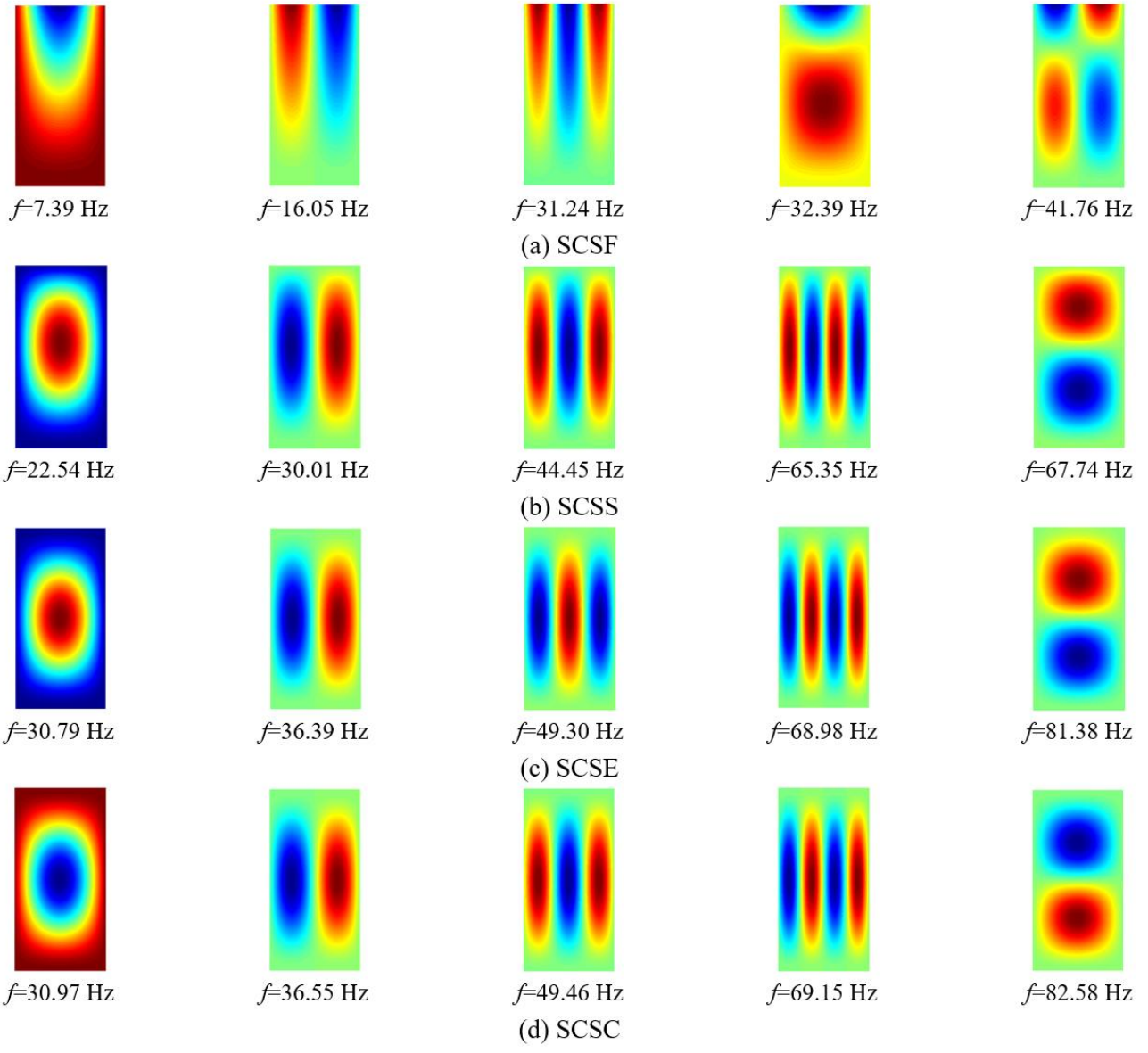

Fig. 6: The first five modes of the structure with b/a=2 under different boundary conditions.

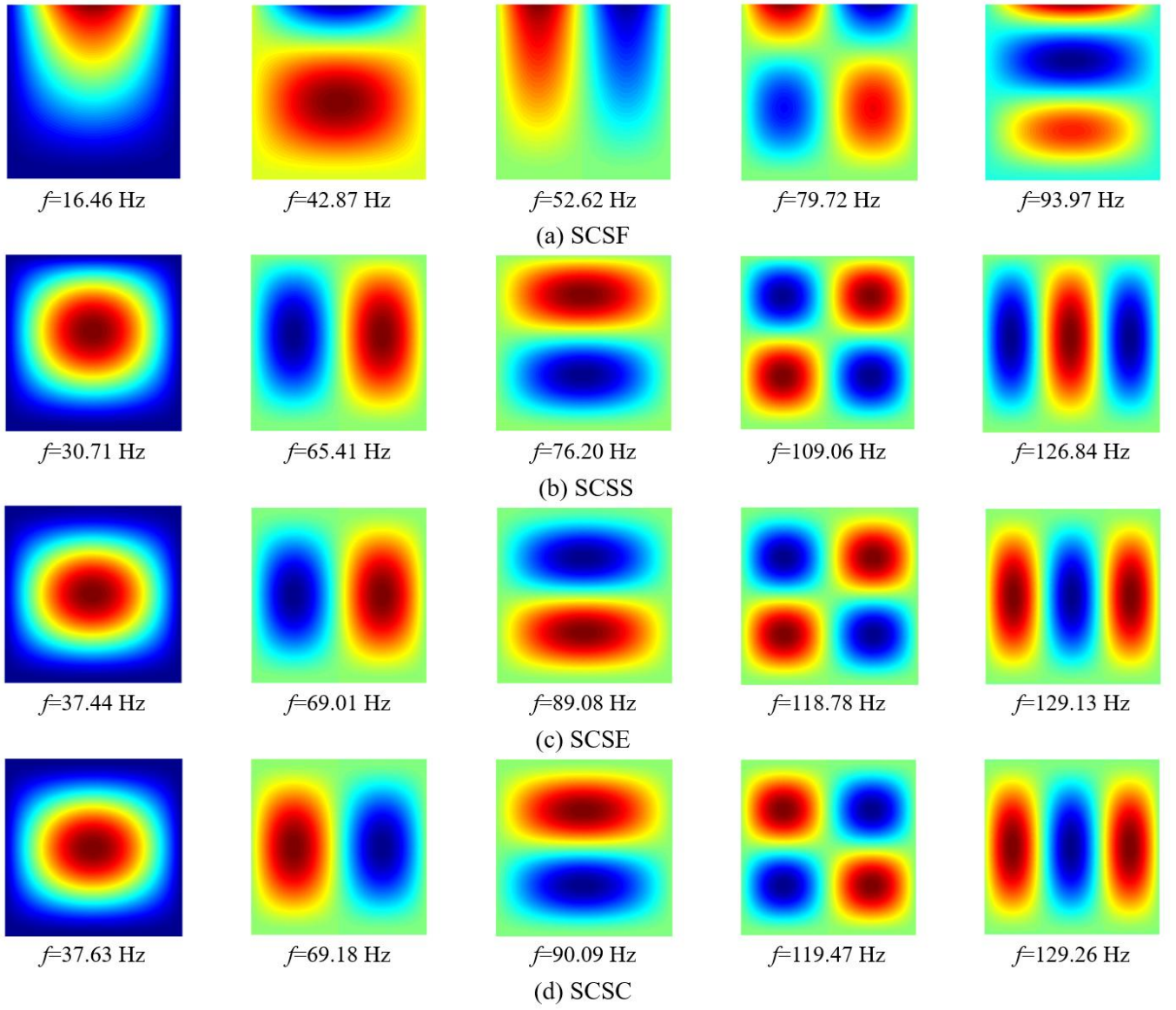

Fig. 7: The first five modes of the structure with b/a=1 under different boundary conditions.

The forced vibration analysis employs excitation at (0.2a, 0.5b) with response monitoring at (0.8a, 0.75b), and the vibration acceleration is converted into a vibration acceleration level to make the data more intuitive and clearer in Eq. (49):

$$L_a=20*\lg(a_1/a_0) \tag{49}$$

where a_1 is the vibration acceleration and a_0 =10^{-6} m/s^2 represents the reference acceleration.

The forced vibration response of the structure with different boundary conditions is shown in Fig. 8, it can be found that the response spectra reveal resonant peaks aligning with natural frequencies. With the weakening of boundary conditions, the peak frequency decreases and the peak count increases within the same frequency range.

4.2 Influence of the structural parameter

Figs. 9 and 10 present the contour map of the structure under SSSS and SCSC boundary conditions with different structural parameters. In the research process, the variation range of their width-to-length ratios is in [1, 5], and thickness-to-length ratios is in [0.01, 0.05]. The rest of the structural parameters of the FGM plates are default. According to the comparative analysis, it can be seen that the increase of thickness-to-length ratio leads to the increase of frequency under both SSSS and SCSC boundary conditions. This is because the increase in thickness directly increases the cross-sectional moment of inertia of the plate, thereby enhancing its bending stiffness. In addition, under the SCSC condition, the increase in thickness has a more significant effect on the natural frequency. This is because the two clamped boundaries provide stronger

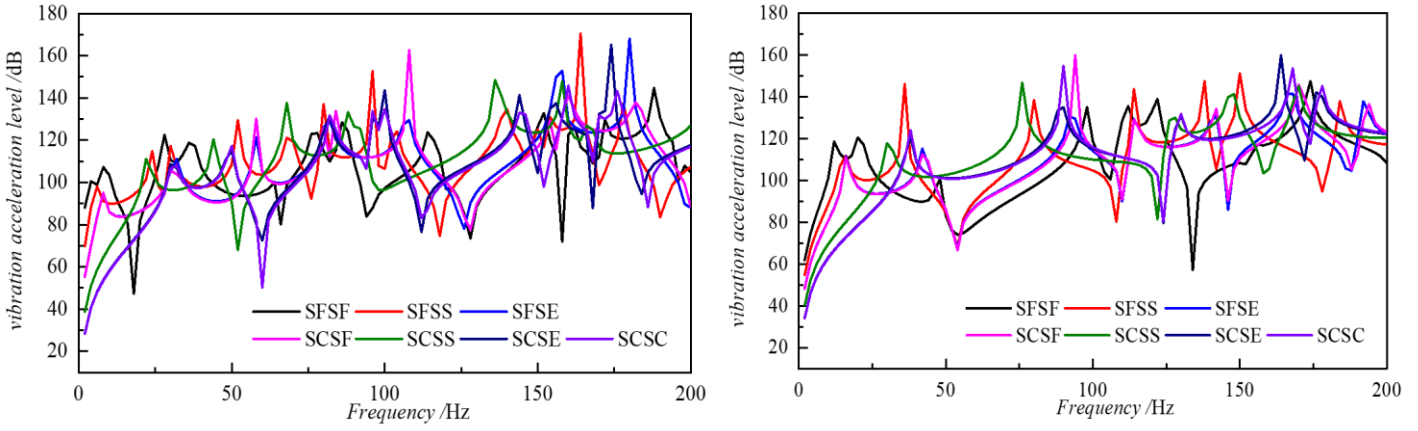

(a) b/a=2 (b) b/a=1

Fig. 8: Forced vibration characteristics of the structure with different boundary conditions.

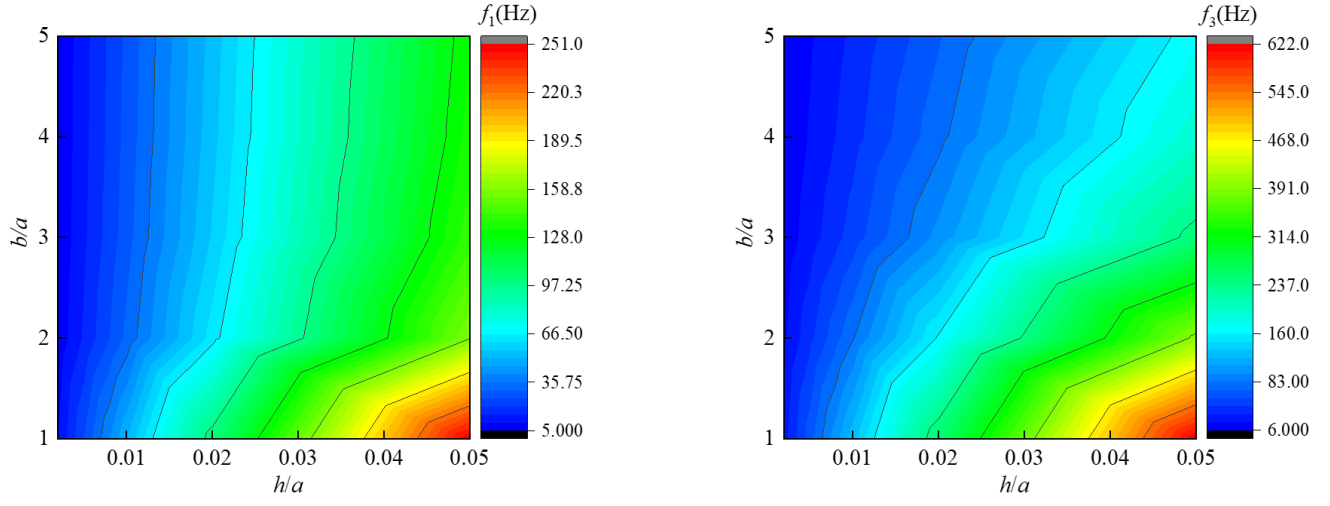

(a) The first order (b) The third order

Fig. 9: Free vibration characteristics of the structure under SSSS boundary condition with different structural parameters.

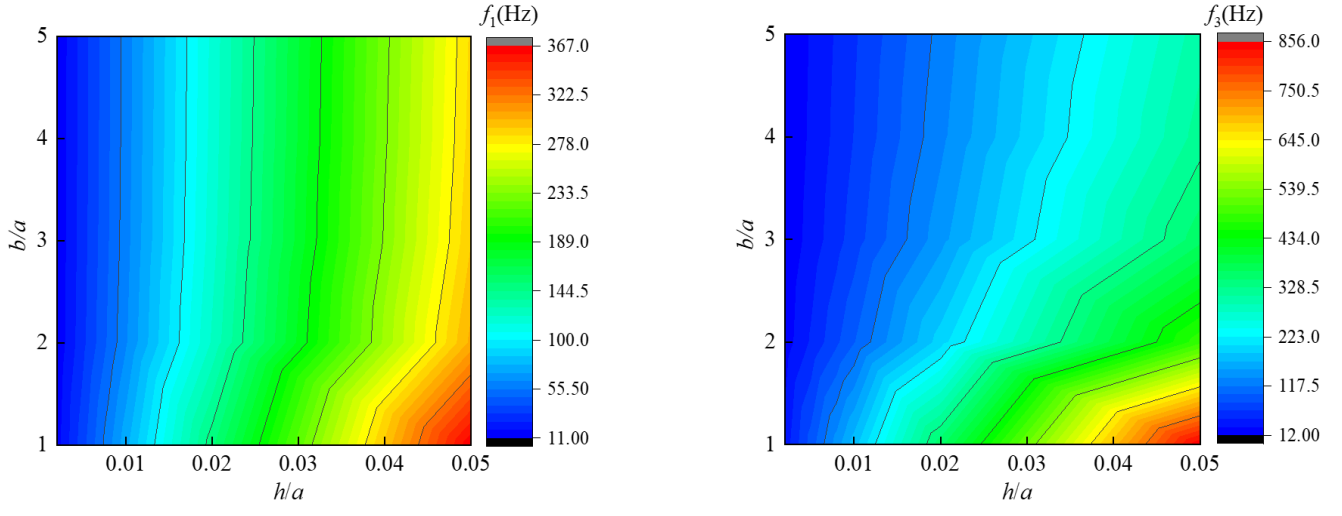

(a) The first order (b) The third order

Fig. 10: Free vibration characteristics of the structure under SCSC boundary condition with different structural parameters.

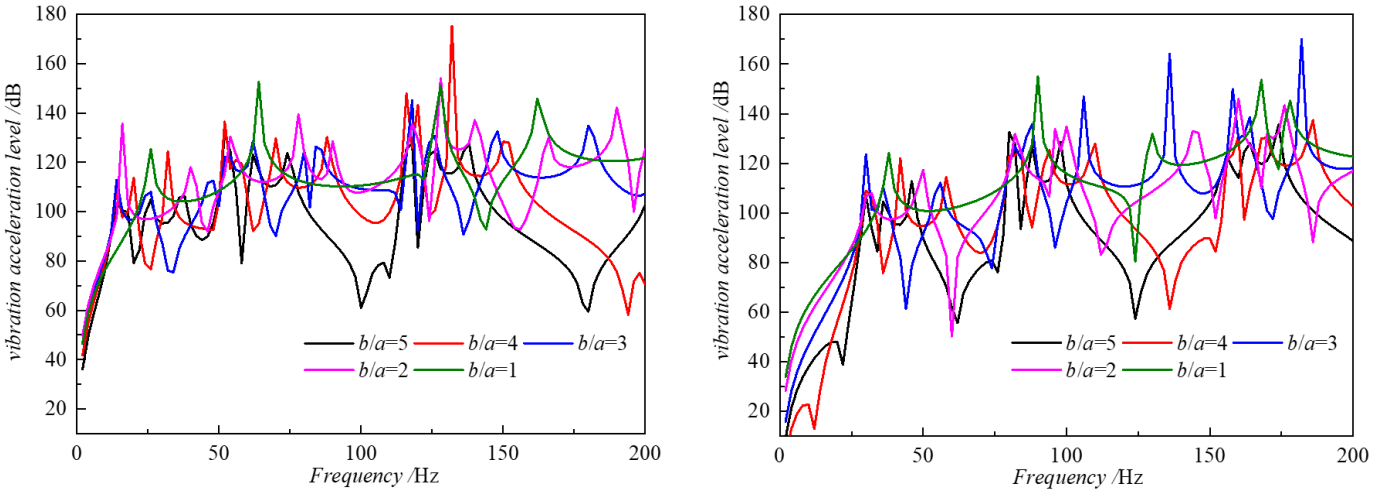

(a) SSSS boundary condition (b) SCSC boundary condition

Fig. 11: Forced vibration characteristics of the structure with different b/a.

rotational constraints and significantly enhance the local stiffness of the plate. Especially in high-order modes, the local stiffness contributes more to the natural frequency. The decrease of width-to-length ratio leads to the increase of natural frequency. When the width of the plate decreases, the stiffness in this direction increases, thus increasing the overall frequency. Under SCSC boundary condition, due to stronger boundary constraints, the decrease of width-to-length ratio has a more obvious effect on the increase of natural frequency.

Fig. 11 delineates the influence of varying width-to-length ratios on the dynamic response of the structure, it can be found that the peak frequency increases and the peak count decreases within the same frequency range with the decrease of width-to-length ratio. This phenomenon indicates that the effective stiffness of the structure will significantly increase with the decrease of width-to-length ratio, thus increasing the vibration frequencies of the FGM plates.

The setting of different thicknesses of structural segments is realized by utilizing domain decomposition method in this study, resulting in modified vibrational behavior. The free vibration response of FGM plates under SCSC boundary condition shows significant dependence on both thickness distribution patterns and power-law exponent p, as quantitatively demonstrated in Table 5 and Fig. 12. In the research process, the thickness ratios of the four segments of the structure are kept consistent while the distribution forms are different, the thickness distribution is set as $h_1/h_2/h_3/h_4$=1/2/2/1,1/1/2/2, 1/2/1/2 and 2/1/1/2, and power-law exponent is in [0, ∞]. Significant variations in dynamic response emerge when altering either the thickness profile or power-law exponent p, as quantitatively demonstrated in the results.

Structural configurations with thicker clamped boundaries exhibit elevated natural frequencies, as evidenced by the

Table 5: Natural frequencies of the structure under SCSC boundary condition with different thickness distribution and power-law exponent.

	Mode	p=0	p=2	p=20	p=50	p=100	p=∞
$h_1/h_2/h_3/h_4$ =1/2/2/1	1	37.469	37.284	36.927	36.005	35.496	35.097
	2	48.920	47.315	48.046	46.974	46.336	45.822
	3	73.670	71.371	72.368	70.742	69.780	69.005
$h_1/h_2/h_3/h_4$ =1/1/2/2	1	42.214	41.983	41.601	40.563	39.990	39.541
	2	53.775	52.000	52.813	51.635	50.935	50.370
	3	74.814	72.482	73.490	71.839	70.863	70.076
$h_1/h_2/h_3/h_4$ =1/2/1/2	1	44.206	43.984	43.565	42.478	41.877	41.406
	2	54.107	52.314	53.137	51.953	51.249	50.680
	3	75.484	73.179	74.154	72.484	71.499	70.704
$h_1/h_2/h_3/h_4$ =2/1/1/2	1	60.357	60.064	59.484	57.997	57.177	56.534
	2	68.323	66.035	67.094	65.602	64.714	63.996
	3	82.865	80.284	81.393	79.568	78.488	77.618

comparison between 2/1/1/2 and 1/2/2/1 thickness distribution. The natural frequencies is largely unaffected by the thickness configurations (1/1/2/2 and 1/2/1/2), as their variation primarily alters only the middle two sections. FGM plates consistently demonstrate intermediate natural frequencies between the two extreme homogeneous cases (p=0 or p=∞), indicating that both material gradation and thickness distribution serve as effective design parameters for vibration characteristic modulation in engineering applications.

4.3 Influence of the elastic foundation

This subsection examines how Winkler-Pasternak foundation parameters influence the vibrational characteristics of FGM plates with two distinct boundary configurations. Four groups of different ($\overline{k_{wt}}$, $\overline{k_{st}}$) are selected, including (0,0), (0,1000), (1000,0) and (1000,1000). The effects of $\overline{k_{wt}}$ and $\overline{k_{st}}$ on the free vibration and dynamic response of FGM plates are shown in Figs. 13 and 14. Clearly, from these figures, demonstrating significant enhancement in mechanical performance when incorporating elastic foundation effects, evidenced by elevated natural frequencies compared to foundation-free cases. Notably, frequency responses show minimal variation between (0,0) and (1000,0) foundation parameters, mirroring the similar behavior observed between (0,1000) and (1000,1000) configurations. The $\overline{k_{st}}$ exhibits greater influence than $\overline{k_{wt}}$, primarily through its constraint effect on transverse plate deflection.

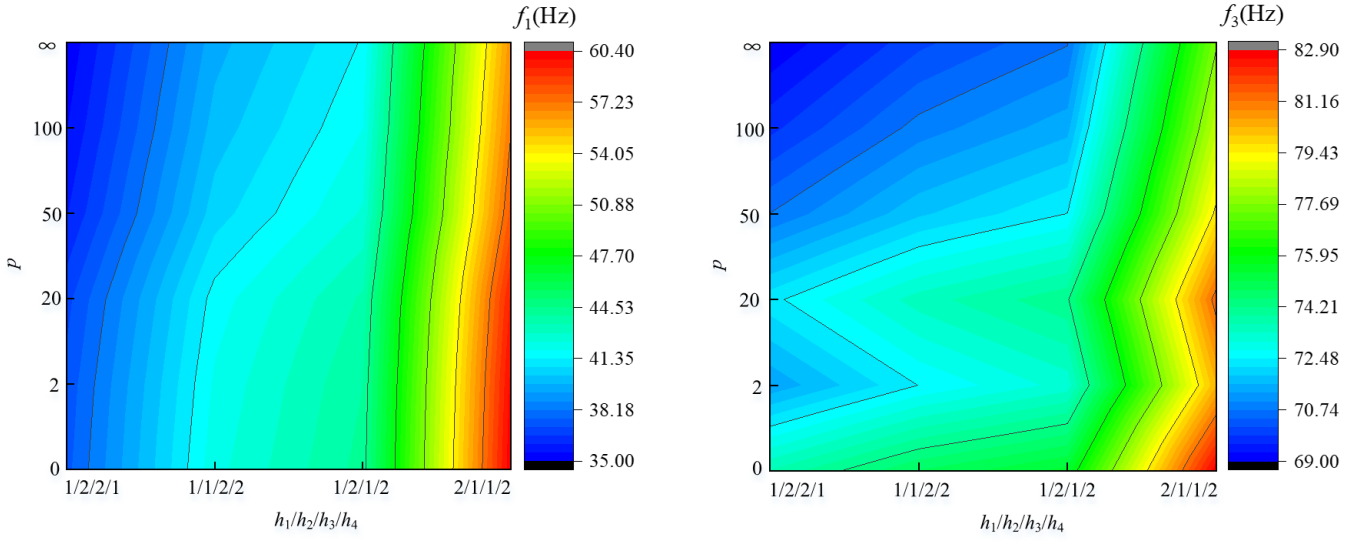

(a) The first order (b) The third order

Fig. 12: Free vibration characteristics of the structure under SCSC boundary condition with different thickness distribution and power-law exponent.

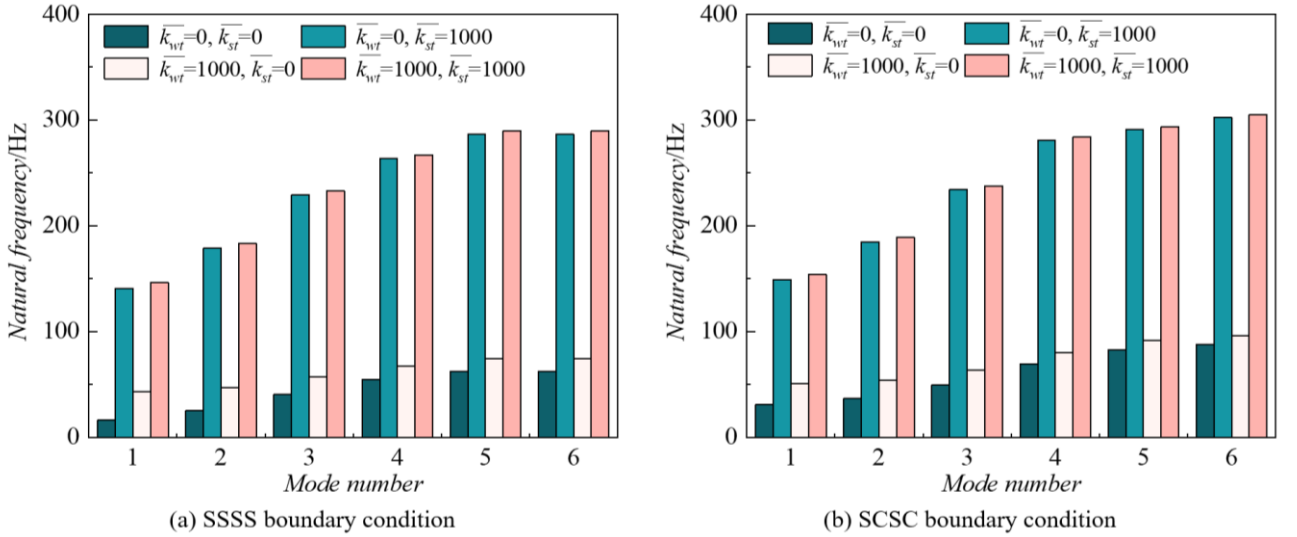

(a) SSSS boundary condition (b) SCSC boundary condition

Fig. 13: Free vibration characteristics of the structure with different Winkler-Pasternak elastic foundations.

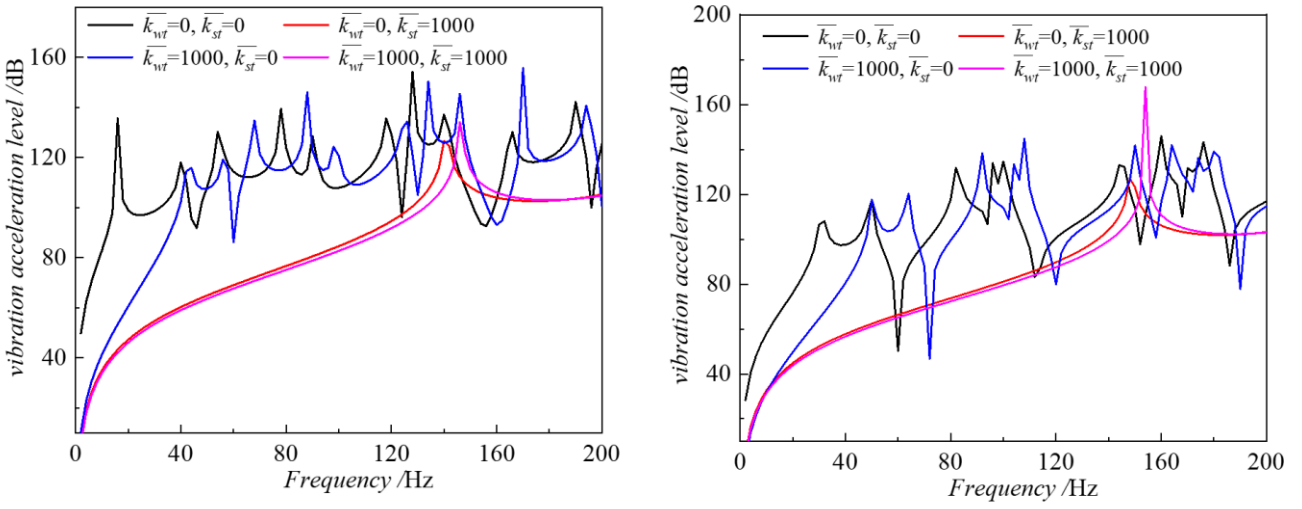

(a) SSSS boundary condition (b) SCSC boundary condition

Fig. 14: Forced vibration characteristics of the structure with different Winkler-Pasternak elastic foundations.

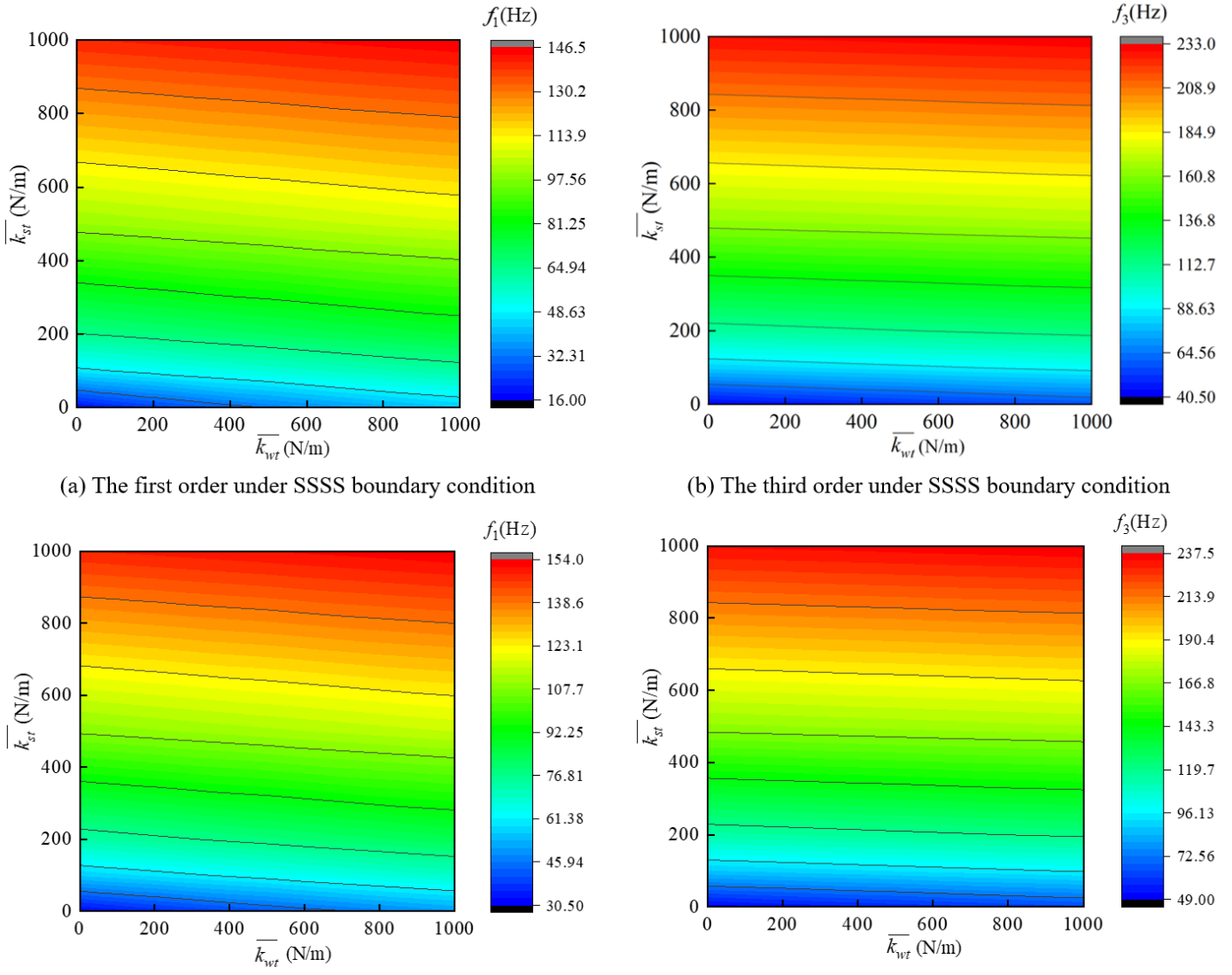

(a) The first order under SSSS boundary condition (b) The third order under SSSS boundary condition

(c) The first order under SCSC boundary condition (d) The third order under SCSC boundary condition

Fig. 15: Comparison of the natural frequencies with varying Winkler-Pasternak elastic foundations.

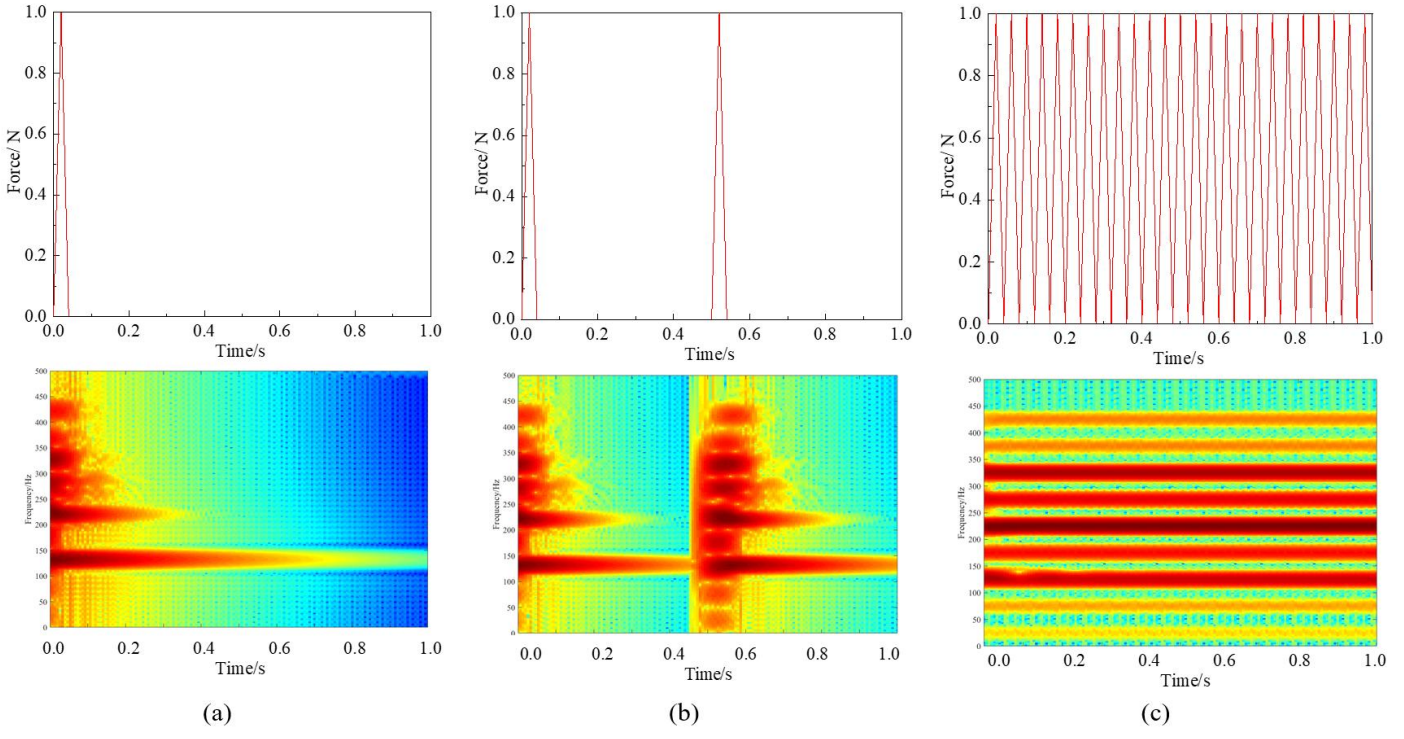

Fig. 16: Vibration characteristics of the structure under different transient excitation load. (a) Vibration response under 1 pulse per second, (b) Vibration response under 2 pulses per second, and (c) Vibration response under 25 pulses per second.

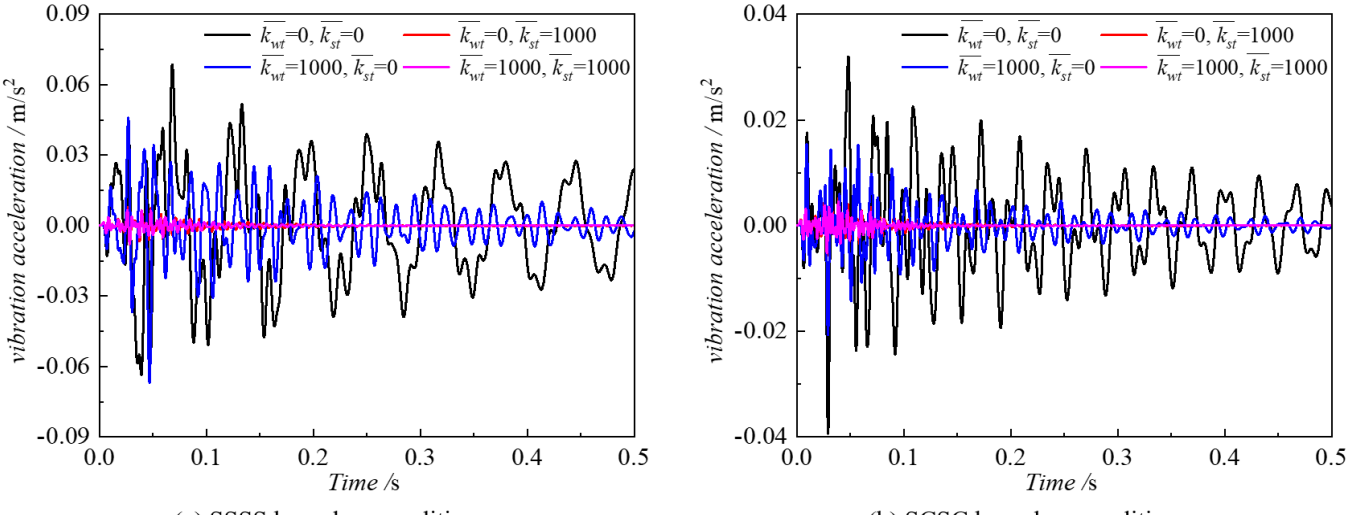

(a) SSSS boundary condition (b) SCSC boundary condition

Fig. 17: Transient vibration characteristics of the structure with different Winkler-Pasternak elastic foundations.

In order to deepen the understanding on the influence of elastic foundation parameters, Fig. 15 presents the comparison of the natural frequencies with varying Winkler-Pasternak elastic foundations. In the research process, the variation range of $\overline{k_{wt}}$ and $\overline{k_{st}}$ is in [0, 1000]. According to the comparative analysis, it can be seen that the natural frequencies of the structure are more sensitive to $\overline{k_{st}}$, which further illustrates that the influence of the $\overline{k_{st}}$ on the potential energy is more obvious.

4.4 Vibration characteristics under transient excitation

In this section, the transient vibration analysis of the structure subjected to external excitation loads is carried out, the excitation point and the assessment point are consistent with the steady forced vibration. The transient vibration characteristics are investigated in Fig. 16 under triangular pulse loading conditions with varying repetition rates (1, 2, and 25 pulses per second). Spectral analysis reveals three key phenomena: (a) The displayed amplitude attenuation reflects the energy dissipation characteristics due to structural

damping under dynamic loads and frequency domain dependence of the structure, the high-frequency vibration has a shorter wavelength and is more significantly affected by dissipation, and the high-frequency component (such as 322 Hz) attenuates faster than the low-frequency component (such as 140 Hz). (b) The broadband frequency component is excited by the transient excitation, and the response peak mainly appears at the natural frequency of the structure (140 Hz, 229 Hz, 286 Hz, 322 Hz, *etc*) and continues to oscillate. (c) The more number of the load cycles, the vibration response will also peak at its excitation frequency and frequency doubling component, such as 25 Hz, 75 Hz, *etc*. it shows that high-frequency repeated load will cause cumulative damage effect.

Fig. 17 exhibits the transient vibration of the structure with different elastic foundations under SSSS and SCSC boundary conditions. The results demonstrate that the period and amplitude of the transient vibration response diminish as the elastic foundation parameters are intensified. In addition, it can also be observed that the change of the $\overline{k_{st}}$ has a more obvious influence on the transient vibration response of the structure.

5. Conclusions

In the present study, the dynamic behavior of FGM plates resting on Winkler-Pasternak elastic foundations was systematically examined. The proposed analytical framework combined domain decomposition techniques, artificial spring boundary modeling and the first-order shear deformation theory to achieve enhanced computational convergence and accuracy, and the dynamic modeling of uniform and stepped structures can be realized. Structural displacement fields were mathematically represented using Jacobi orthogonal polynomial expansions, with vibration characteristics subsequently analyzed through the Rayleigh-Ritz method. Time-dependent response solutions were obtained by employing the Newmark-β numerical integration approach. Validation against from published numerical data confirmed the reliability of the proposed method. The dynamic behavior of FGM plates exhibited strong dependence on both geometric parameters and boundary constraints. Structural stiffness demonstrated an inverse relationship with width-to-length ratio, while enhanced boundary restraints contribute to improved mechanical performance. Comparative analysis demonstrated that elastic foundation support substantially elevated natural frequencies relative to unsupported configurations. Furthermore, the results underscored the potential of employing optimized thickness gradation and material property distribution to mitigate vibration in practical engineering applications.

Acknowledgements

This study was funded by National Natural Science Foundation of China (52401368, 52401383) and Postdoctoral Fellowship Program of CPSF (GZC20233427).

Conflict of Interest

There is no conflict of interest.

Supporting Information

Applicable.

CRediT Statement

Xianghong Huang: Writing–review & editing. **Luyue Xi**: Writing–original draft. **Cong Gao**: Conceptualization and Methodology. **Yuchen Fan**: Data curation and Validation. **Yuan Zhou**: Investigation and Software.

References

[1] D. S. Cho, J. H. Kim, T. M. Choi, B. H. Kim, N. Vladimir, Free and forced vibration analysis of arbitrarily supported rectangular plate systems with attachments and openings, *Engineering Structures*, 2018, **171**, 1036-1046, doi: 10.1016/j.engstruct.2017.12.032.

[2] A. Sharma, N. Mani, R. Bhardwaj, K. Kumar, Thermal vibration of rectangle plate with two-dimensional circular thickness effect, *Mathematical Problems in Engineering*, 2022, **2022**, 9744671, doi: 10.1155/2022/9744671.

[3] Z. Hu, Y. Shi, C. Guo, J. Du, R. Li, New analytical solutions for free vibration of cracked functionally graded rectangular plates, *AIAA Journal*, 2024, **62**, 3960-3977, doi: 10.2514/1.J063936.

[4] M. Derakhshani, S. Hosseini-Hashemi, M. Fadaee, An analytical closed-form solution for free vibration of stepped circular/annular Mindlin functionally graded plate, *Arxiv Preprint Arxiv:1804.10583*, 2018, 1-11, doi: 10.48550/arXiv.1804.10583.

[5] F. Najafi, M. H. Shojaeefard, H. Saeidi Googarchin, Nonlinear low-velocity impact response of functionally graded plate with nonlinear three-parameter elastic foundation in thermal field, *Composites Part B: Engineering*, 2016, **107**, 123-140, doi: 10.1016/j.compositesb.2016.09.070.

[6] N. Belbachir, A. Tounsi, M. A. Al-Osta, A new HSDT for buckling and free vibration behavior of cross-ply laminated composite plates resting on elastic foundation, *Computers and Concrete*, 2025, **35**, 29-41, doi: 10.12989/cac.2025.35.1.029.

[7] H. Akhavan, S. H. Hashemi, H. R. D. Taher, A. Alibeigloo, S. Vahabi, Exact solutions for rectangular Mindlin plates under in-plane loads resting on Pasternak elastic foundation. Part II: Frequency analysis, *Computational Materials Science*, 2009, **44**,

951-961, doi: 10.1016/j.commatsci.2008.07.001.
[8] M. H. Yas, A. Jodaei, S. Irandoust, M. Nasiri Aghdam, Three-dimensional free vibration analysis of functionally graded piezoelectric annular plates on elastic foundations, *Meccanica*, 2012, **47**, 1401-1423, doi: 10.1007/s11012-011-9525-y.
[9] N. Kolarevic, M. Nefovska-Danilovic, M. Petronijevic, Dynamic stiffness elements for free vibration analysis of rectangular Mindlin plate assemblies, *Journal of Sound and Vibration*, 2015, **359**, 84-106, doi: 10.1016/j.jsv.2015.06.031.
[10] R. Kırışık, Yüksel, Free vibration analysis of a rectangular plate with kelvin type boundary conditions, *Shock and Vibration*, 2007, **14**, 447-457, doi: 10.1155/2007/307575.
[11] C. Wu, S. Liu, Y. Chen, Applying the principle of mixed variables solve the problems of forced vibration of the calculating rectangular plate by uniform load, *Applied Mechanics and Materials*, 2011, **71**, 1715-1719, doi: 10.4028/www.scientific.net/amm.71-78.1715.
[12] C. Lü, Z. Zhang, W. Chen, Free vibration of generally supported rectangular Kirchhoff plates: State-space-based differential quadrature method, *International Journal for Numerical Methods in Engineering*, 2007, **70**, 1430-1450, doi: 10.1002/nme.1929.
[13] I. Ramu, S. C. Mohanty, Study on free vibration analysis of rectangular plate structures using finite element method, *Procedia Engineering*, 2012, **38**, 2758-2766, doi: 10.1016/j.proeng.2012.06.323.
[14] M. K. Kwak, S. Han, Free vibration analysis of rectangular plate with a hole by means of independent coordinate coupling method, *Journal of Sound and Vibration*, 2007, **306**, 12-30, doi: 10.1016/j.jsv.2007.05.041.
[15] K. Kim, B. Kim, T. Choi, D. Cho, Free vibration analysis of rectangular plate with arbitrary edge constraints using characteristic orthogonal polynomials in assumed mode method, *International Journal of Naval Architecture and Ocean Engineering*, 2012, **4**, 267-280, doi: 10.2478/IJNAOE-2013-0095.
[16] T. Zhao, T. Ye, Y. Chen, G. Jin, Z. Liu, Single domain Chebyshev spectral method for analyses of the vibroacoustic characteristics of baffled irregularly shaped plates, *Journal of Sound and Vibration*, 2024, **592**, 118627, doi: 10.1016/j.jsv.2024.118627.
[17] T. Ye, T. Zhao, Y. Chen, G. Jin, X. Ma, Z. Liu, Vibroacoustic analysis of baffled plate with elastic boundary conditions in heavy fluid near free surface based on Chebyshev spectral approach, *Ocean Engineering*, 2025, **332**, 121399, doi: 10.1016/j.oceaneng.2025.121399.
[18] P. Singhatanadgid, P. Taranajetsada, Vibration analysis of stepped rectangular plates using the extended Kantorovich method, *Mechanics of Advanced Materials and Structures*, 2016, **23**, 201-215, doi: 10.1080/15376494.2014.949922.
[19] X. Su, E. Bai, A. Chen, Symplectic superposition solution of free vibration of fully clamped orthotropic rectangular thin plate on two-parameter elastic foundation, *International Journal of Structural Stability and Dynamics*, 2021, **21**, 2150122, doi: 10.1142/s0219455421501224.
[20] L. Srubshchik, I. Herskowitz, I. Peckel, E. Potetyunko, Static and dynamic buckling of a compressed narrow rectangular plate on an elastic foundation, *Mechanical Systems and Control*, 2008, **11**, 349-356, doi: 10.1115/imece2008-68384.
[21] Z. Celep, Z. Özcan, A. Güner, Elastic triangular plate dynamics on unilateral Winkler foundation: Analysis using Chebyshev polynomial expansion for forced vibrations, *Journal of Mechanical Science and Technology*, 2025, **39**, 65-79, doi: 10.1007/s12206-024-1207-5.
[22] Y. Xiao, C. Yang, Free vibration analysis for disconnected thin rectangular plate with four free edges on nonlinear elastic foundation, *Applied Mechanics and Materials*, 2011, **52**, 1309-1314, doi: 10.4028/www.scientific.net/amm.52-54.1309.
[23] Y. Xiao, C. Yang, H. Hu, Nonlinear forced vibration analysis for thin rectangular plate on nonlinear elastic foundation, *Applied Mechanics and Materials*, 2012, **204**, 4716-4721, doi: 10.4028/www.scientific.net/amm.204-208.4716.
[24] H. Hajheidari, H. R. Mirdamadi, Free and transient vibration analysis of an un-symmetric cross-ply laminated plate by spectral finite elements, *Acta Mechanica*, 2012, **223**, 2477-2492, doi: 10.1007/s00707-012-0719-8.
[25] P. M. Phuc, N. T. Kim Khue, New finite modeling of free and forced vibration responses of piezoelectric FG plates resting on elastic foundations in thermal environments, *Shock and Vibration*, 2021, **2021**, 6672370, doi: 10.1155/2021/6672370.
[26] M. C. Srivastav, B. Rajak, A. K. Tiwari, H. K. Sharma, R. Kumar, J. Singh, Analysis of free vibration characteristics of porous FGM skew plate using meshfree approach, *Multiscale and Multidisciplinary Modeling, Experiments and Design*, 2024, **7**, 6245-6261, doi: 10.1007/s41939-024-00576-3.
[27] M. C. Srivastava, S. Singh, B. Rajak, H. K. Sharma, R. Kumar, J. Singh, Buckling response of two-directional skew FGM plate resting on elastic foundation: A RBFMC approach, *Computers and Concrete*, 2025, **35**, 357-367, doi: 10.12989/cac.2025.35.4.357.
[28] D. Singh, S. Rai, A. Gupta, Vibration analysis of sandwich functionally graded material plate with cut-outs using artificial neural network technique, *Thin-Walled Structures*, 2024, **202**, 112072, doi: 10.1016/j.tws.2024.112072.
[29] T. I. Thinh, T. M. Tu, N. Van Long, Free vibration of a horizontal functionally graded rectangular plate submerged in fluid medium, *Ocean Engineering*, 2020, **216**, 107593, doi: 10.1016/j.oceaneng.2020.107593.

[30] S. Hosseini-Hashemi, H. Rokni Damavandi Taher, H. Akhavan, M. Omidi, Free vibration of functionally graded rectangular plates using first-order shear deformation plate theory, *Applied Mathematical Modelling*, 2010, **34**, 1276-1291, doi: 10.1016/j.apm.2009.08.008.

[31] M. Javani, Y. Kiani, M. R. Eslami, Application of generalized differential quadrature element method to free vibration of FG-GPLRC T-shaped plates, *Engineering Structures*, 2021, **242**, 112510, doi: 10.1016/j.engstruct.2021.112510.

[32] S. Ghosh, A. K. Bhowmick, S. Haldar, Combined effect of mass and two-parameter elastic foundation on the free vibration characteristics of laminated composite plates using a FSDT-based finite element method, *Journal of Vibration Engineering & Technologies*, 2025, **13**, 283, doi: 10.1007/s42417-025-01851-4.

[33] P. Van Vinh, A novel modified nonlocal strain gradient theory for comprehensive analysis of functionally graded nanoplates, *Acta Mechanica*, 2025, **236**, 173-204, doi: 10.1007/s00707-024-04131-6.

[34] L. T. Son, P. V. Vinh, N. V. Chinh, H. M. Sedighi, High-frequency temperature-dependent vibration of nonlocal functionally graded sandwich nanoplates resting on elastic foundations, *Mechanics of Advanced Materials and Structures*, 2025, **32**, 957-978, doi: 10.1080/15376494.2024.2358108.

[35] L. T. Son, M. O. Belarbi, A. Tounsi, H. Ziou, M. Avcar, P. Van Vinh, Nonlocal vibration analysis of functionally graded sandwich nanoplates resting on general viscoelastic foundations, *Mechanics of Advanced Materials and Structures*, 2025, 1-18, doi: 10.1080/15376494.2025.2521729.

[36] P. Van Vinh, A. M. Zenkour, Vibration analysis of functionally graded sandwich porous plates with arbitrary boundary conditions: a new general viscoelastic Winkler–Pasternak foundation approach, *Engineering with Computers*, 2025, 1-29, doi: 10.1007/s00366-025-02106-2.

[37] D. Shi, H. Zhang, Q. Wang, S. Zha, Free and forced vibration of the moderately thick laminated composite rectangular plate on various elastic winkler and Pasternak foundations, *Shock and Vibration*, 2017, **2017**, 7820130, doi: 10.1155/2017/7820130.

[38] Q. Wang, D. Shi, Q. Liang, F. Pang, Free vibration of four-parameter functionally graded moderately thick doubly-curved panels and shells of revolution with general boundary conditions, *Applied Mathematical Modelling*, 2017, **42**, 705-734, doi: 10.1016/j.apm.2016.10.047.

[39] Q. Wang, X. Cui, B. Qin, Q. Liang, J. Tang, A semi-analytical method for vibration analysis of functionally graded (FG) sandwich doubly-curved panels and shells of revolution, *International Journal of Mechanical Sciences*, 2017, **134**, 479-499, doi: 10.1016/j.ijmecsci.2017.10.036.

[40] X. Zhao, Y. Y. Lee, K. M. Liew, Free vibration analysis of functionally graded plates using the element-free kp-Ritz method, *Journal of Sound and Vibration*, 2009, **319**, 918-939, doi: 10.1016/j.jsv.2008.06.025.

[41] X. Q. He, T. Y. Ng, S. Sivashanker, K. M. Liew, Active control of FGM plates with integrated piezoelectric sensors and actuators, *International Journal of Solids and Structures*, 2001, **38**, 1641-1655, doi: 10.1016/S0020-7683(00)00050-0.

[42] H. Zhang, R. Zhu, D. Shi, Q. Wang, A simplified plate theory for vibration analysis of composite laminated sector, annular and circular plate, *Thin-Walled Structures*, 2019, **143**, 106252, doi: 10.1016/j.tws.2019.106252.

[43] Q. Wang, K. Choe, J. Tang, C. Shuai, A. Wang, Vibration analyses of general thin and moderately thick laminated composite curved beams with variable curvatures and general boundary conditions, *Mechanics of Advanced Materials and Structures*, 2020, **27**, 991-1005, doi: 10.1080/15376494.2018.1503760.

[44] H. Hu, R. Zhong, Q. Wang, X. Shi, Spectro-geometry dynamic analysis of FG-GPLRC cylindrical shell with periodically embedded dynamic vibration absorbers, *Thin-Walled Structures*, 2024, **203**, 112243, doi: 10.1016/j.tws.2024.112243.

[45] K. K. Pradhan, S. Chakraverty, Free vibration of Euler and Timoshenko functionally graded beams by Rayleigh–Ritz method, *Composites Part B*: *Engineering*, 2013, **51**, 175-184, doi: 10.1016/j.compositesb.2013.02.027.

[46] Ö. Civalek, Free vibration of carbon nanotubes reinforced (CNTR) and functionally graded shells and plates based on FSDT *via* discrete singular convolution method, *Composites Part B*: *Engineering*, 2017, **111**, 45-59, doi: 10.1016/j.compositesb.2016.11.030.

[47] K. M. Liew, L. X. Peng, S. Kitipornchai, Buckling analysis of corrugated plates using a mesh-free Galerkin method based on the first-order shear deformation theory, *Computational Mechanics*, 2006, **38**, 61-75, doi: 10.1007/s00466-005-0721-2.

[48] T. Ye, G. Jin, Z. Su, Y. Chen, A modified Fourier solution for vibration analysis of moderately thick laminated plates with general boundary restraints and internal line supports, *International Journal of Mechanical Sciences*, 2014, **80**, 29-46, doi: 10.1016/j.ijmecsci.2014.01.001.

[49] V. L. Nguyen, M. T. Tran, S. Limkatanyu, J. Rungamornrat, Free vibration analysis of rotating FGP sandwich cylindrical shells with metal-foam core layer, *Mechanics of Advanced Materials and Structures*, 2023, **30**, 3318-3331, doi: 10.1080/15376494.2022.2073410.

[50] Z. Qin, Z. Yang, J. Zu, F. Chu, Free vibration analysis of rotating cylindrical shells coupled with moderately thick annular plates, *International Journal of Mechanical Sciences*, 2018, **142**, 127-139, doi: 10.1016/j.ijmecsci.2018.04.044.

[51] J. Liu, X. Deng, Q. Wang, R. Zhong, R. Xiong, J. Zhao, A unified modeling method for dynamic analysis of GPL-reinforced

FGP plate resting on Winkler-Pasternak foundation with elastic boundary conditions, *Composite Structures*, 2020, **244**, 112217, doi: 10.1016/j.compstruct.2020.112217.
[52] M. S. Qatu, Cylindrical shells, *Vibration of Laminated Shells and Plates*, Amsterdam: Elsevier, 2004, 259-320, doi: 10.1016/b978-008044271-6/50008-9.
[53] Q. Wang, Q. Yang, R. Zhong, Dynamics analysis of Gyroid lattice plates under moving loads, *Advances in Engineering Software*, 2025, **211**, 104038, doi: 10.1016/j.advengsoft.2025.104038.
[54] X. Li, W. Zhang, X. Yang, L. Song, A unified approach of free vibration analysis for stiffened cylindrical shell with general boundary conditions, *Mathematical Problems in Engineering*, 2019, **2019**, 4157930, doi: 10.1155/2019/4157930.
[55] H. Matsunaga, Free vibration and stability of functionally graded plates according to a 2-D higher-order deformation theory, *Composite Structures*, 2008, **82**, 499-512, doi: 10.1016/j.compstruct.2007.01.030.
[56] S. Pradyumna, J. N. Bandyopadhyay, Free vibration analysis of functionally graded curved panels using a higher-order finite element formulation, *Journal of Sound and Vibration*, 2008, **318**, 176-192, doi: 10.1016/j.jsv.2008.03.056.
[57] K. Y. Lam, C. Wang, X. He, Canonical exact solutions for Levy-plates on two-parameter foundation using Green's functions, *Engineering Structures*, 2000, **22**, 364-378, doi: 10.1016/S0141-0296(98)00116-3.